



Lake ice simulation using a 3D unstructured grid model

Yinglong Joseph Zhang¹ · Chin Wu² · Joshua Anderson² · Sergey Danilov³ · Qiang Wang³ · Yuli Liu² · Qian Wang⁴

Received: 28 November 2022 / Accepted: 28 March 2023 / Published online: 13 April 2023
© Springer-Verlag GmbH Germany, part of Springer Nature 2023

Abstract

We develop a single-class ice and snow model embedded inside a 3D hydrodynamic model on unstructured grids and apply it to lake studies using highly variable mesh resolution. The model is able to reasonably capture the ice fields observed in both small and large lakes. For the first time, we attempt simulation of ice processes on very small scales (~ 1 m). Physically sound results are obtained at the expense of moderately increased computational cost, although more rigorous validation nearshore is needed due to lack of observation. We also outline challenges on developing new process-based capabilities for accurately simulating nearshore ice.

Keywords Ice simulation · Unstructured grids · SCHISM · Great Lakes

1 Introduction

Lake ice plays an important role in lake circulation and biogeochemical processes (White et al. 2012; Fujisaki et al. 2013). Majority of the current generations of ice models (Bouillon et al. 2013) are concentration based implemented in the Eulerian framework, although attempts have been made to utilize progressive damage models used in rock mechanics expressed in the Lagrangian framework (Bouillon and Rampal 2015) and also discrete element method (West et al. 2022).

Most lake ice models are adapted from sea ice models with minor modifications in parameterizations (e.g., White et al. 2012; Bai et al. 2020; Li et al. 2021). Aside from the large lakes (e.g., the Great Lakes), a popular efficient approach for modeling

lake ice is based on one-dimensional models (Mironov et al. 2010; Smirnova et al. 2016; Xiao et al. 2016; Benjamin et al. 2022). These one-dimensional lake models appear to be sufficient for modeling small lakes but have limitations for modeling ice and hydrodynamics in large lakes. We, therefore, focus on a coupled 2D ice and 3D hydrodynamic model in this paper.

A main challenge in lake ice studies is to capture very small-scale ice processes as found in harbors and ports. To the best of our knowledge, this challenge has not been directly addressed due to formidable difficulty related to our understanding of small-scale processes, in addition to numerical stability.

In this paper, we apply an unstructured-grid, single class (in terms of ice thickness) ice and snow model embedded inside a widely used 3D hydrodynamics model SCHISM (schism.wiki; Zhang et al. 2016) to model seasonal development of lake ice in the Great Lake region, including both a small lake (Lake Mendota) and a large lake (Lake Superior). Although a multi-class ice model based on CICE/Icepack (Hunke et al. 2015) is also available inside SCHISM, it is more instructive to address the numerical challenges such as using very high mesh resolution with a simpler single-class model first before adding more ice physics. Note that the high resolution is not meant as a way to resolve individual ice floes. We will not detail the model skill for other physical variables such as the water temperature (except for a brief comparison of lake surface temperature (LST)), as we have demonstrated that in previous publications (e.g., Zhang et al. (2015) for Lake Mendota) and will do so in upcoming

This article is part of the Topical Collection on the *12th International Workshop on Modeling the Ocean (IWMO), Ann Arbor, USA, 25 June – 1 July 2022*

Responsible Editor: Jia Wang, Joanna Staneva

✉ Yinglong Joseph Zhang
yjzhang@vims.edu

¹ Virginia Institute of Marine Science, Gloucester Point, VA, USA

² University of Wisconsin-Madison, Madison, WI, USA

³ Alfred Wegener Institute Helmholtz Center for Polar and Marine Research, Bremerhaven, Germany

⁴ School of Oceanography, Shanghai Jiao Tong University, Shanghai, China

publications (e.g., Anderson et al. (to be submitted) for Lake Superior).

In Section 2, we describe the major observation datasets and model setup we use in this paper. Section 3 details the ice model validation for two lakes. The ice results including sensitivity for Lake Superior are further analyzed in Section 4, where we will also present some preliminary results for application of the ice model to harbors and rivers using very fine local resolution and outline the challenges on developing new process-based capabilities for accurately simulating nearshore ice. Section 5 summarizes the paper and also provides future direction.

2 Observation and model setup

Ice observation data is usually scarcer than the standard hydrodynamic data, and, therefore, we use two sets of observations (ice mass and ice concentration) taken from two lake systems in this paper in order to evaluate the performance of our ice model.

The ice mass (thickness) data were collected for a small dimictic lake near Madison, Wisconsin. Lake Mendota, with a mean depth of 12.7 m and maximum depth of 25.3 m, has a surface area of 39.4 km², a shoreline length of about 34 km, and a maximum fetch of 9.8 km (Kitchell 1992). Although located in the Great Lakes region, Lake Mendota is not directly connected to any of the five Great Lakes. It freezes over each year in the winter. The ice data are available at the North Temperate Lakes Long-Term Ecological Research (NTL-LTER) Program website (<http://lter.limnology.wisc.edu/index.html>). Intensive sampling was conducted weekly

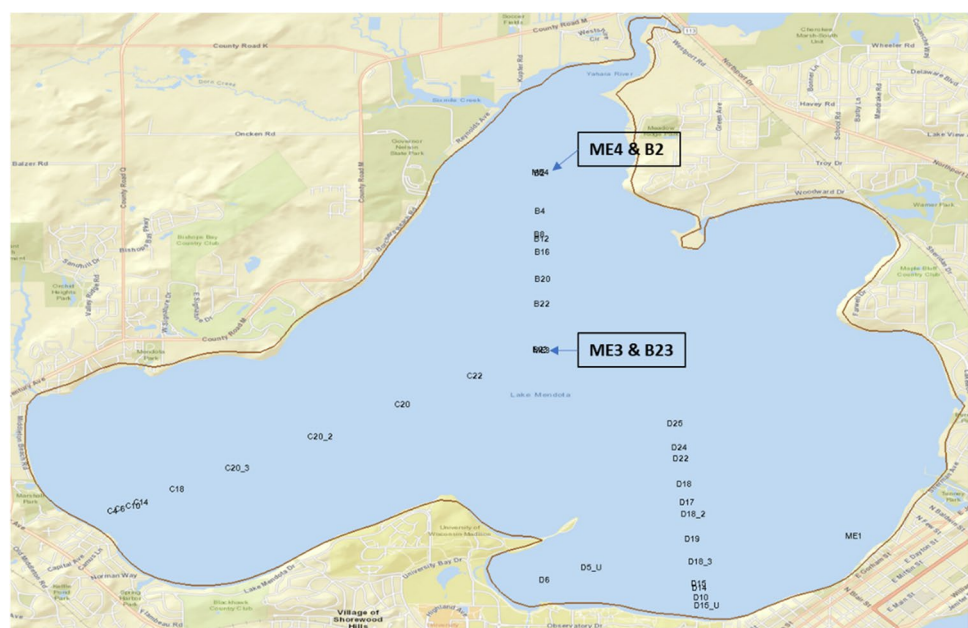
from January 14 to March 30, 2010 on Lake Mendota when the ice was safe to walk on, using a Kovacs Mark III core drill to collect ~27 ice cores, which yielded a total of 165 measurements of ice and snow thickness (Fig. 1). The station locations used in comparison are shown in Fig. 1. In addition, thermistor chains were deployed in Lake Mendota at three locations at water depths of 5 m (D5), 15 m (D15), and 25 m (D25) (Fig. 1). Under-ice water temperatures were recorded from January 30 to March 5, 2010, which is used to initialize the model temperature in this paper.

For the Lake Superior system, which is the largest (containing 10% of the total surface freshwater on earth; Matheson and Munawar 1978) and least perturbed by human activities among the Laurentian Great Lakes (White et al. 2012), we use the Great Lakes Surface Environmental Analysis (GLSEA) data to assess the modeled ice concentration. Ice dynamics are an integral part of the physical processes in this temperate lake, and annual freezing usually starts around early December and ice cover persists until April/May in the next year, with maximum strength reached around mid-March. The water tends to be well mixed during this period.

Although some scattered coring data is available for this system as well (Titze and Austin (2016) presented data for 2014–2015), we have not been able to obtain such data for any recent years. Nonetheless, the ice concentration data from GLSEA allows a comprehensive assessment of the ice model in a large area.

The modeling system used in this paper is an open-source unstructured-grid-based 3D model (SCHISM; schism.wiki; Zhang et al. 2016) that incorporates an ice component, derived from a well-validated community ocean-ice model

Fig. 1 Lake Mendota showing the ice coring and thermistor chain locations



(FESOM: finite-volume sea ice-ocean model; Wang et al. 2014). Both SCHISM and the ice model allow multi-scale physics on variable resolution; in the vertical dimension, a highly flexible vertical gridding system (LSC²; Zhang et al. 2015) is used to optimally place resolution where it is needed, with variable number of layers at different depths. The vertical grid allows shaved cells and a single layer to be used; the latter effectively morphs the model to 2DH (2D depth averaged) configuration locally. To address the challenges of scaling for the application cases shown in this paper, two algorithmic modifications were made to the ice model as described below.

Unstructured meshes are generated for the two lakes using the best available digital elevation models (DEMs). Shown in Fig. 2 is the Superior mesh, with resolution ranging from ~ 5 km (in the deeper basin) to ~ 20 m near some coastal structures nearshore. The mesh has ~ 34,000 nodes and ~ 63,000 elements. The Lake Mendota mesh is substantially smaller with 1639 nodes and 3064 elements. In the vertical dimension, we use 1–37 layers, and the average number of layers for Lake Superior is only 8, which makes the model very efficient (it finishes 1 year of simulation in 1 day on 80 cores) using a non-split time step of 100 s for Lake Superior. For simplicity, we use for both lakes a uniform bottom friction coefficient of 0.001, turbulence closure scheme of *k-ε*, and transport solver of TVD² (Ye et al. 2016). Note that we have previously demonstrated that the turbulence mixing in the lakes can be captured by the Generic Length-scale model embedded inside SCHISM (Zhang et al. 2015). The air–water momentum and heat exchanges follow the bulk aerodynamic model of Zeng et al. (1998). However, different atmospheric forcings are used for the two lakes: for the 2009–2010 simulation of Mendota, we use Climate Forecast System Reanalysis (CFSRv1; <https://cfs.ncep.noaa.gov/cfsr/>); for the 2018–2020 simulation of Superior, we use the newer High-Resolution Rapid Refresh (HRRR; <https://rapidrefresh.noaa.gov/hrrr/>), which is not available for earlier years. HRRR has a nominal resolution of 3 km with hourly prediction, which is much finer than CFSRv1.

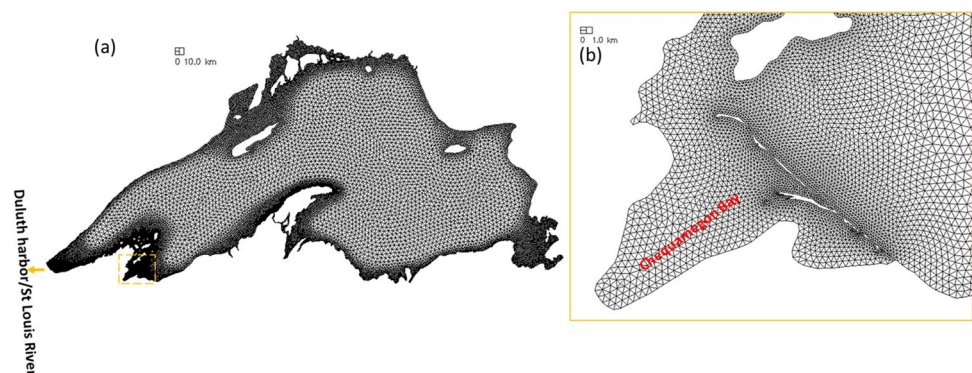
The initial temperature used in the model came from observation: station measurement for Lake Mendota or GLSEA remote sensed lake surface temperature (LST) for Lake Superior. We started the model in late fall when both the temperature stratification and ice extent are minimal. The ice model uses a single class of ice and snow, a modified elastic-visco-plastic (mEVP; Bouillon et al. 2013) solver for momentum, and a flux-corrected transport (FCT; Wang et al. 2014) solver for the ice transport. Ice thermodynamics formulation is based on Parkinson and Washington (1979). Standard values for ice and snow albedos are used here: 0.85/0.75 for dry or frozen snow/ice, and 0.75/0.66 for melting snow/ice, respectively.

Since we will be dealing with very high-resolution meshes (cf. Section 4.2), two algorithmic modifications were necessary in the ice model. Neither of these are exclusively related to the lake environment. The first change is related to mEVP, which uses a pseudo-time solver for VP rheology (Bouillon et al. 2013). Essentially, an iterative scheme is used to bypass the stringent CFL stability limit with potential downside of divergence to the original VP state. We use 200 iterations in this paper as increasing it to 500 did not seem to change the results. More importantly, the two weights (α and β as in Bouillon et al. 2013) must be sufficiently large to satisfy the CFL, especially on fine meshes. Therefore, an adaptive scheme (aEVP) is proposed for such cases:

$$\alpha = \beta = C/\tanh(BA/\Delta t_{ice}) \tag{1}$$

where *A* is the element area, *C* is the minimum, and *B* is an adjustable coefficient that controls how quickly α and β depart from their minimum, Δt_{ice} is the time step used in the ice model (taken to be the main model time step of 100 s in this paper). Except for the case in Section 4.2 with very fine mesh (down to 1 m), we found that a constant value (e.g., 200) for α and β is sufficient. On very fine meshes, we found that the adaptive scheme had to be used to avoid instability (Section 4.2). The second algorithmic change is related to FCT in the inundation zone: the lower-order solution is

Fig. 2 **a** Unstructured grid for Lake Superior, with **b** zoom-in showing high resolution (~ 20 m) used nearshore in Chequamegon Bay. The mesh is later extended to include Duluth harbor and St Louis River watershed (i.e., west of the boundary in (a); cf. Section 4.2)



used with maximum monotonicity constraint in this region to ensure stability.

3 Model validation

In this section, we assess the model's ability to simulate ice mass and concentration in the two lakes.

3.1 Lake Mendota case

The simulation starts from an ice-free time (Oct 28, 2009) and lasts 180 days; the lake becomes essentially ice free after ~160 days (March 27, 2010) (Figs. 3 and 5). The model's ability to capture the temperature variation and stratification over each season has been demonstrated in Zhang et al. (2015). The comparison of the ice thickness at the ~27 stations is shown in Fig. 3, and all of the ~165 time-space measurements are compared in Fig. 4. Overall,

the model is able to capture the gradual freezing and rapid melting phases well. The ice thickness reaches its maximum around days 118–146 (Feb. 1 to March 1). The modeled ice seems to melt a little too fast compared to the observation (Fig. 3), and the ice thickness seems to mostly bias high except at a few stations during melting (Figs. 3 and 4). The overall RMSE is 8 cm, compared to the maximum thickness of ~50 cm, suggesting a satisfactory performance.

The model results suggest that the freezing starts on Dec 12, 2009 and melting process finished around April 5, 2010. Between Jan. 2 and Jan. 26, 2010 (days 66 and 90 in Fig. 5), the entire lake is essentially frozen. There is a brief melting period between days 50 and 60 (Fig. 5) when the air temperature hovers above 0 degrees for a sustained period (Fig. 5). The averaged ice velocity during the ice cover period (Fig. 6) suggests that the ice mostly moves from the nearshore toward the lake center. Due to the confined geometry, the velocity is generally small.

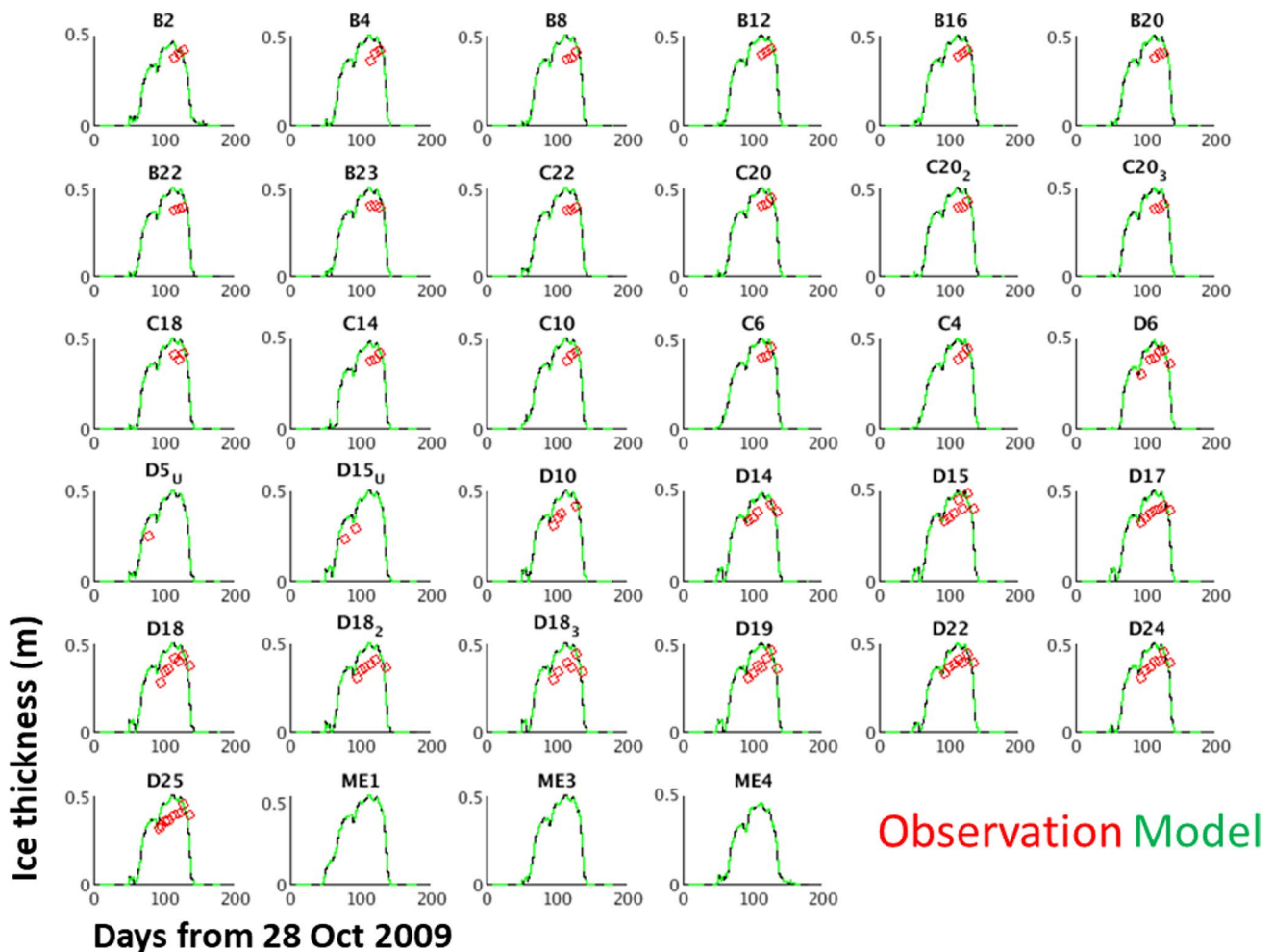


Fig. 3 Comparison of ice thickness at multiple stations (cf. Figure 1). Note that observation data is missing at some stations

Fig. 4 Scattered diagram for the ice thickness comparison. The red line represents a perfect match

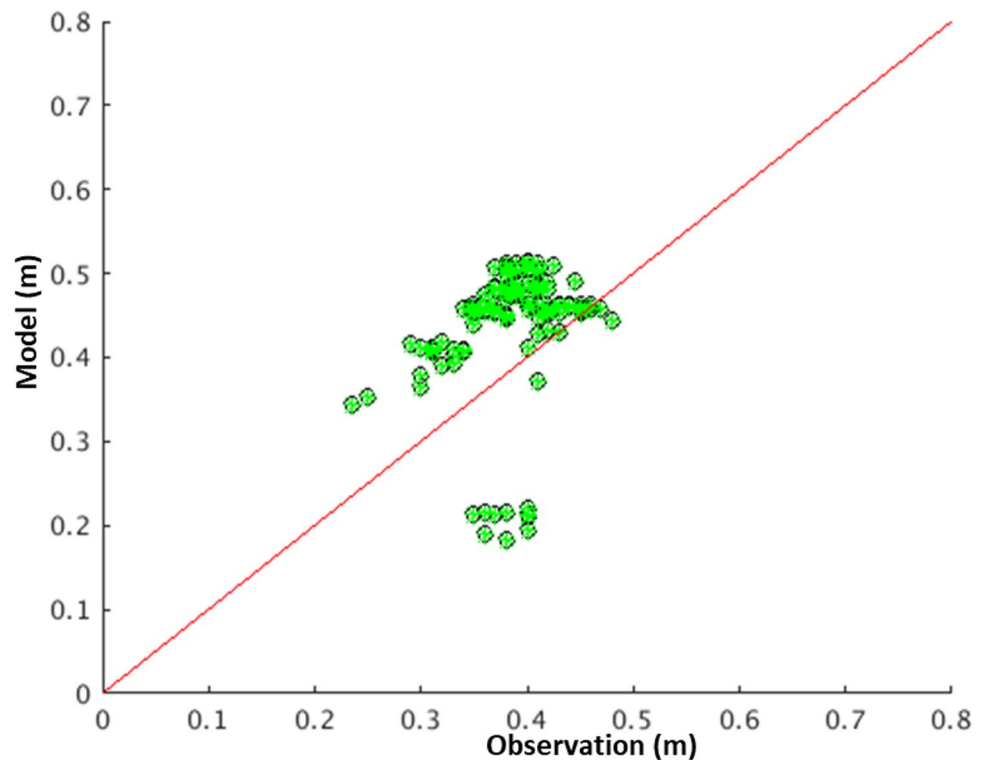
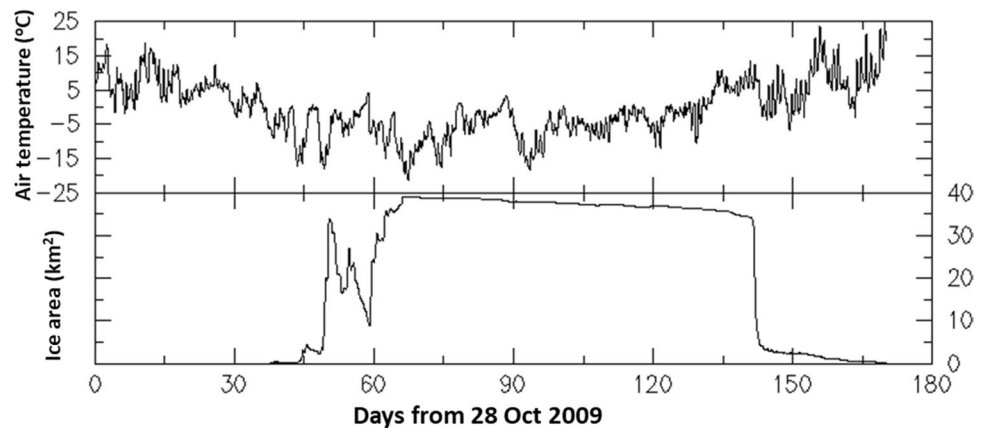


Fig. 5 Time history of air temperature (at the center of the lake) and total ice area. A cut-off threshold of 15% for the ice concentration is used to calculate the total ice area



3.2 Lake Superior case

Ice cover period in Lake Superior usually starts in December and ends in May of each year but exhibits remarkable inter-annual variability (Fig. 7). Of the 3 recent years, 2020 has minimum coverage, while 2018 and 2019 show similar maximum but very different durations (~60 days of near-max coverage in 2018 and ~20 days for 2019) (Fig. 7a–c). The ice area here is defined as places where the ice concentration exceeds 15% and is calculated in the same way for the model and observation in each cell or mesh element over the entire lake. The calculated ice thicknesses (average over all areas with ice concentration exceeding 15%) largely

follow the same trend as concentration, albeit with a phase lag similar to White et al. (2012). The inter-annual variability of ice thickness is large: Even though the maximum area is similar between 2018 and 2019 (Fig. 7a, b), the average ice thickness is twice in 2018 (Fig. 7d, e) due to a prolonged cold spell in that year. Atmospheric forcing (air temperature and solar radiation, etc.) is found to be the main cause for the ice cover variability, as the initial lake temperature (on Dec. 1 of the preceding years) is similar across the 3 years.

The model is able to capture the intra- and inter-annual variation of the ice coverage well (Fig. 7a–c). In particular, it accurately captures the timing of the freezing phase, and the maximum extent is also reasonably simulated including

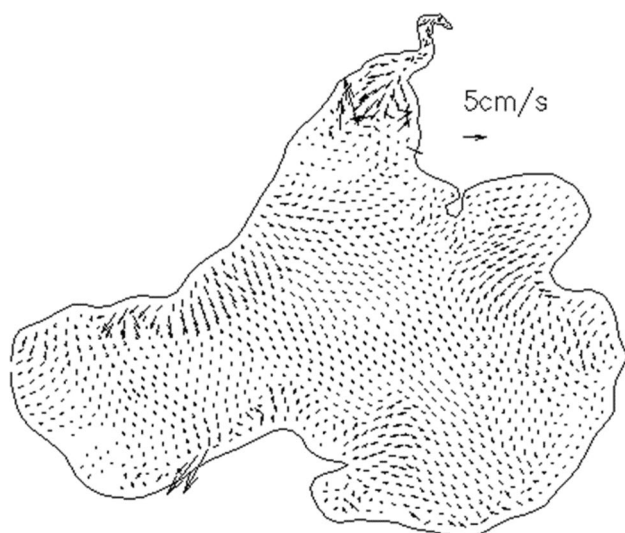


Fig. 6 Averaged ice velocity in the ice cover period (Days 45 to 170)

some rapid melting-refreezing events due to large swings in the air temperature (Figs. 7 and 9). The modeled melting phase also agrees reasonably with observation until near the end, when it tends to melt too fast (Fig. 7). Of the 3 years simulated, 2020 has both the smallest ice coverage and, incidentally, the worst error metrics (Fig. 7). These findings are corroborated by the snapshot comparisons during the 3 phases (Fig. 8). Since the melting usually starts from the

center of the lake and occurs last in nearshore areas (Fig. 8), the errors near the end of the melting phase are most likely from the underestimation nearshore. A potential error source may come from the errors in the heat budget derived from HRRR during the ice melting period; this is especially so because the results from White et al. (2012) for other years (using different atmospheric sources) suggest the opposite trend to ours in delayed melting. On the other hand, the high temporal and spatial resolution as in HRRR allows us to capture high-frequency variations in the ice field (Figs. 7 and 9).

Consistent with the faster-than-reality melting in the model, the simulated lake surface temperature (LST) after ice melt biases higher than GLSEA by ~ 1.3 °C on average, although the spatial variation of LST is well captured (Fig. 10).

4 Discussion

We will focus on the Lake Superior case in this section and skip the sensitivity discussion for Lake Mendota as it is much smaller in size and thus exhibits much-less heterogeneity. We first discuss the ice field from the 2019 simulation including small-scale features and show some sensitivity results. We then show preliminary results from an ice simulation that includes the Duluth harbor in very high resolution (~ 1 m).

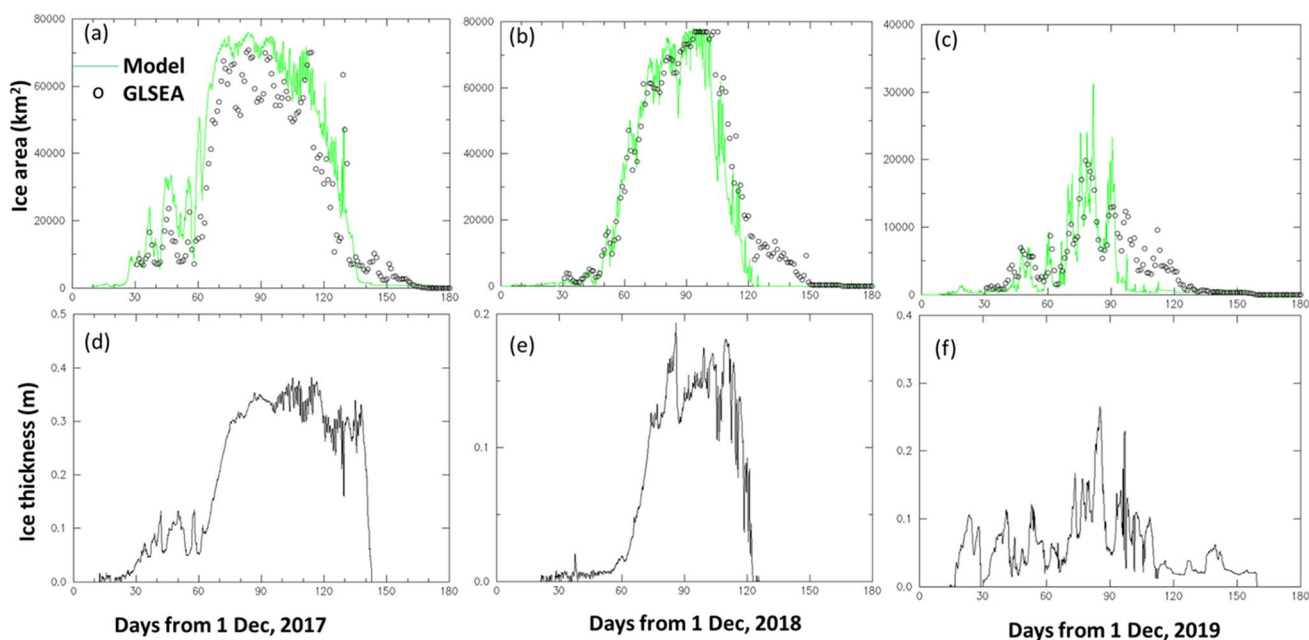


Fig. 7 a–c Comparisons of total ice area (defined as ice concentration exceeding 15%) in Lake Superior in 2018–2020 (starting from December of 2017–2019, respectively). d–f averaged ice thickness in the same 3 years. The Wilmot scores for the 3 years are 0.95, 0.96,

and 0.78, and the correlation coefficients are 0.94, 0.95, and 0.71, respectively. The scores are calculated during the ice-covering periods

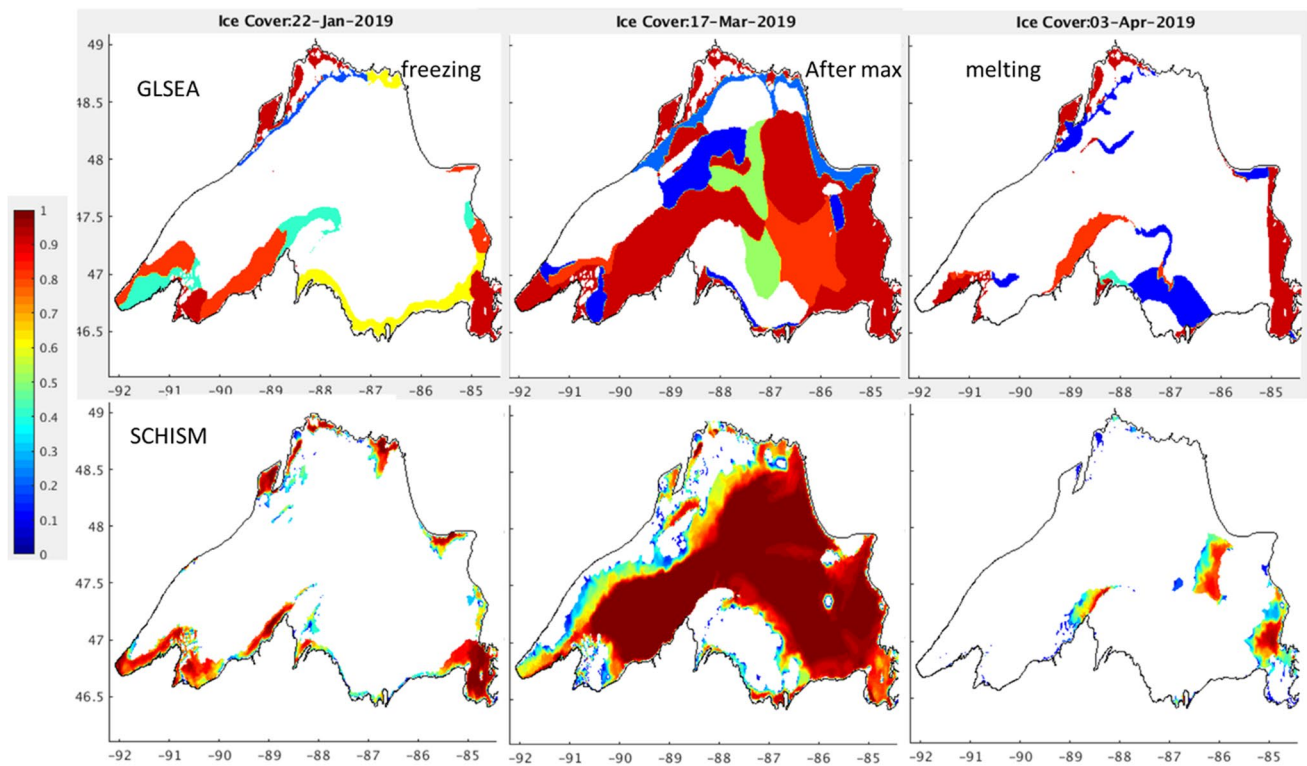


Fig. 8 Snapshot comparisons of ice concentration between GLSEA observation (top row) and model (bottom row) during 3 phases: freezing, near max, and melting in 2019. The model is doing well during

the first 2 phases but melts faster. See Supplemental Material for an animation for the modeled ice concentration. The white space indicates the ice-free areas

4.1 Ice simulation results in Lake Superior

The simulated ice concentration and deformation rate fields are shown in Fig. 11. The measure of deformation rate is composed of the invariants of the strain rate tensor:

$$\Delta = \left[(u_x + v_y)^2 + \frac{(u_x - v_y)^2 + (u_y + v_x)^2}{e^2} \right]^{1/2} \quad (2)$$

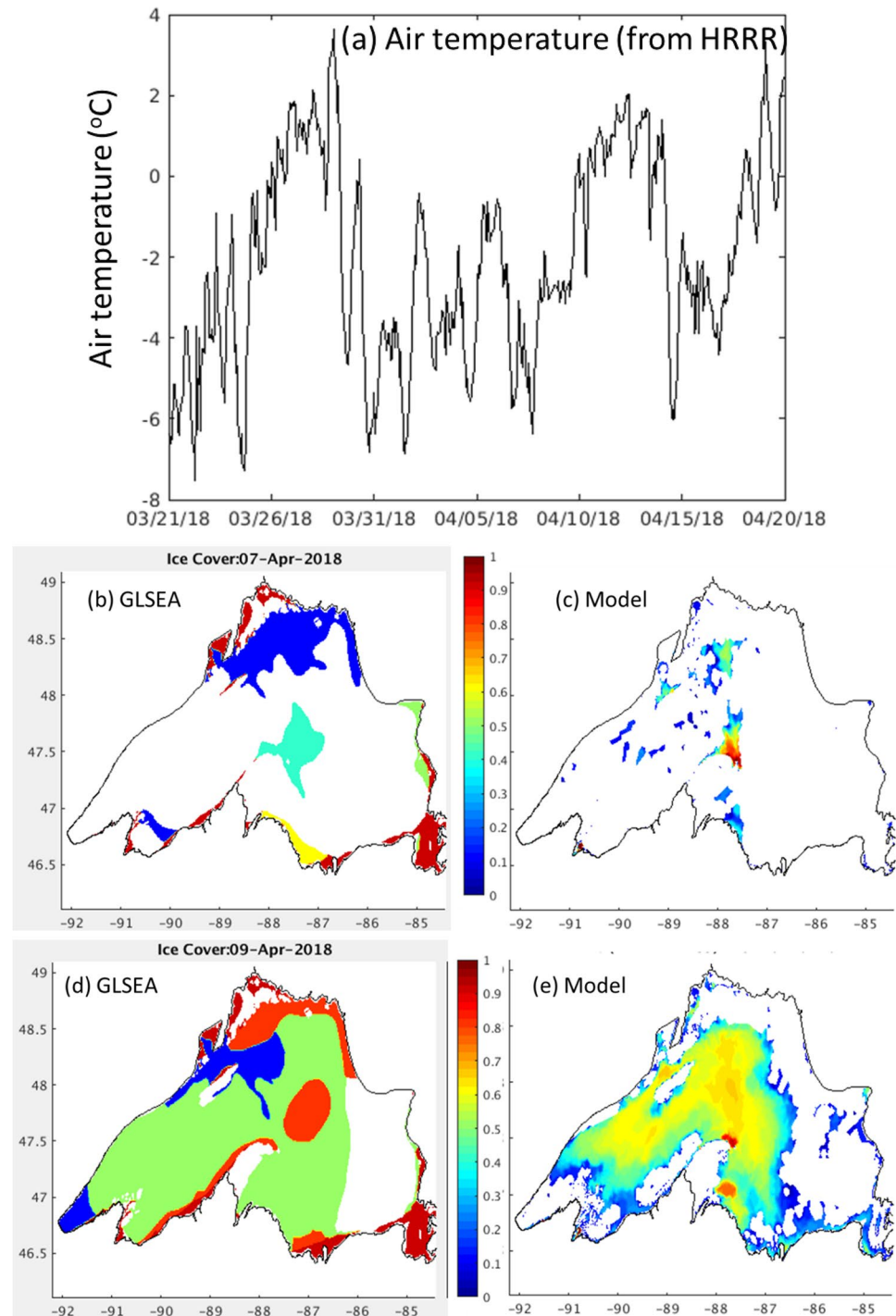
where (u, v) are horizontal ice velocities and $e = 2$ is the ellipse aspect ratio. Δ is an important field and is often used as an indicator of the capability of sea ice rheology in simulating deformation features (Hutter and Losch 2020; Bouchat et al. 2022). Besides, in an EVP-like sea ice model, it is an indicator of the absence of numerical noise. Δ is usually shown in log scale and is usually very small when the concentration is smaller than ~ 0.7 , and the ice exhibits plastic behavior. The Δ field also indicates some fine-scale features, especially nearshore (Fig. 11b, d). The Δ field does not show any noise, except perhaps in some high-resolution parts (Fig. 11d). However, since the ice concentration is far from 1 in those areas, the internal ice stress is hardly playing

a big role there. Correspondingly, the ice velocity is shown to converge nearshore (Fig. 12), resulting in ridging behavior there.

The sensitivity of the ice to the mEVP parameters (α, β) is found to be mostly subtle (Fig. 13). Some minor differences in Δ can be seen in the southeastern area close to shore, which has resulted in small differences in the ice mass there (Fig. 13). The nominal resolution in the deeper depths is 5 km, and the finest resolution nearshore for this mesh is ~ 20 m. A constant value for α, β seems acceptable for this mesh to guarantee the convergence of the ice results.

The ice results are, however, very sensitive to the initial lake temperature. As shown in Fig. 14, a small error in it (± 1 °C) would result in large errors in the total predicted ice area. This is especially true for the freezing phase (Fig. 14). With a colder initial temperature, the maximum and melting phases are similar to the reference simulation (Fig. 14). Interestingly, the more rapid freezing did not seem to substantially delay the melting (Fig. 14). With a warmer initial temperature, however, the ice area appears too small throughout the ice cover period (Fig. 14).

Fig. 9 The rapid melting and refreezing events in 2018. **a** Air temperature during March–April 2018; **b, d** GLSEA observation for ice concentration on April 7 and 9, respectively; **c, e** modeled ice concentration. The white space indicates the ice-free areas



4.2 Exploratory work on ice modeling on very fine meshes

Kimmritz et al. (2017) suggest that the mEVP solver may underestimate the ice strength when the mesh resolution is very high. This is due to the divergence of mEVP results from the “true” VP state, unless a prohibitive number of iterations is used. Implicit solvers like Zhang and Hibler

(1997) share a similar issue of non-convergence with non-linear iterative solvers. The non-convergence, however, may be tolerable for practical applications (Kimmritz et al. 2017).

To the best of our knowledge, none of the previous ice models have been applied to the type of resolution used here, and it is therefore useful to explore their behavior in this extreme case for future development. Strictly speaking, very fine mesh resolution may violate continuum assumption of

Fig. 10 Comparison of LST in 2019 at the end of 180-day simulation between **a** GLSEA observation and **b** model

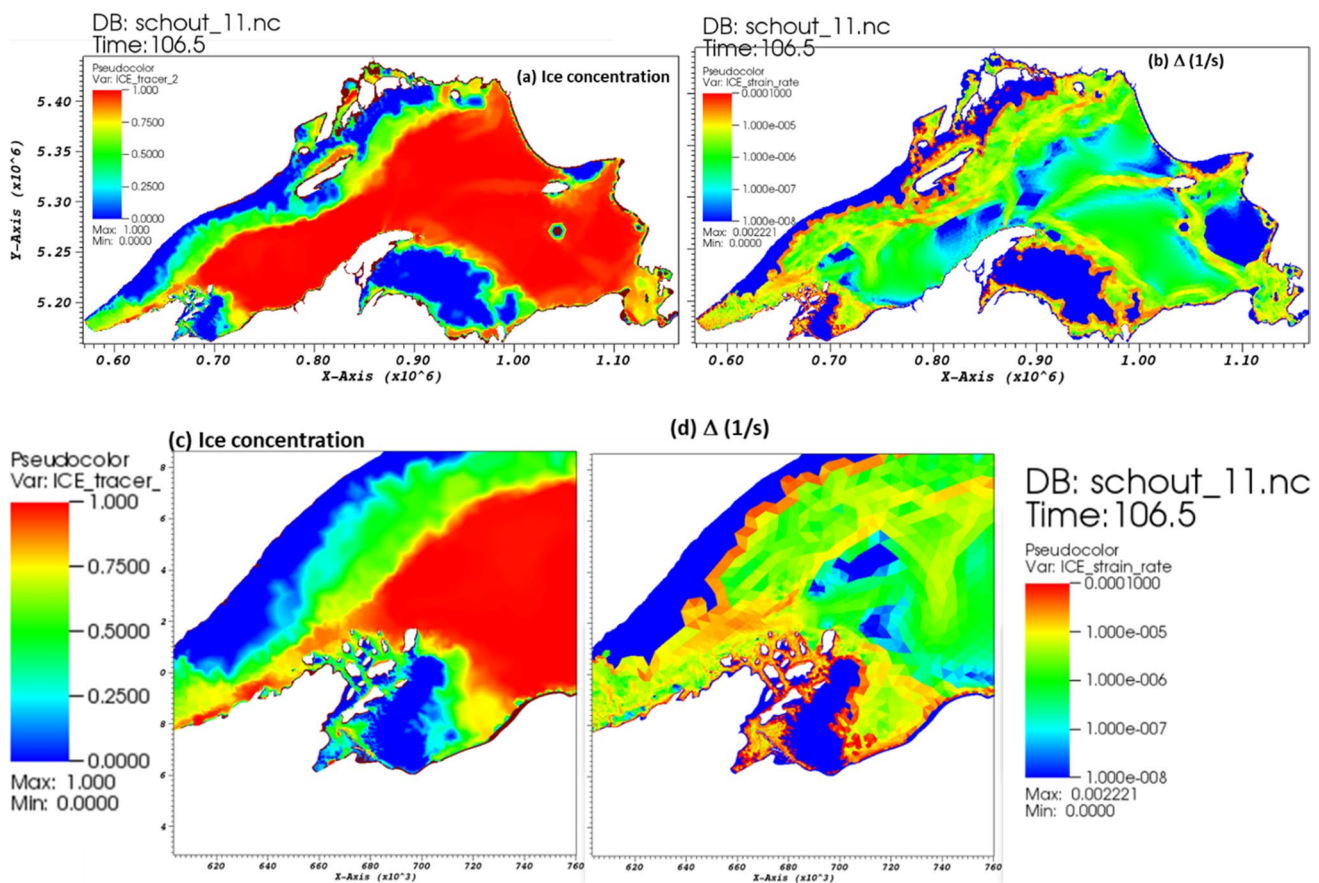
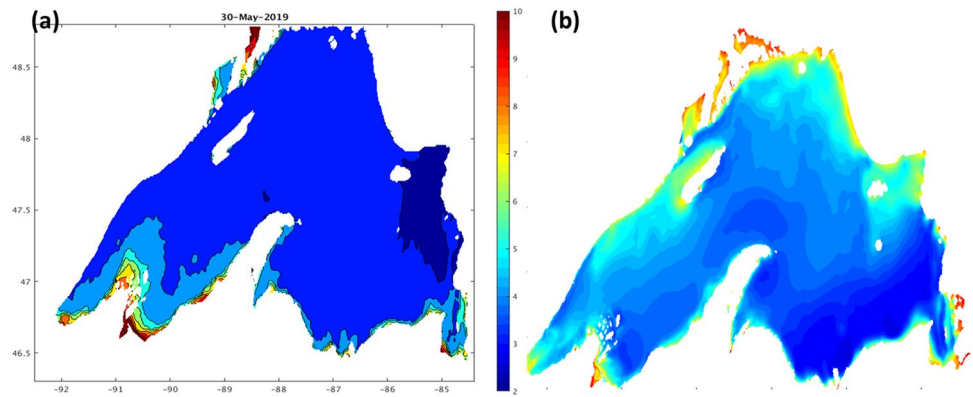


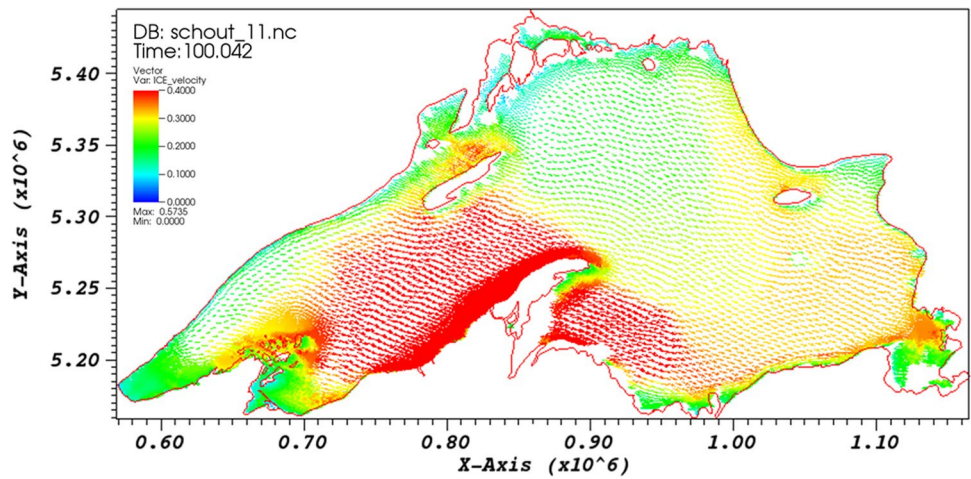
Fig. 11 **a** Ice concentration and **b** Δ in Lake Superior with **c**, **d** zoom-in in the Chequamegon Bay near ice maximum in 2019 (March 17)

ice floes (with size ~ 100 m or larger) in the Eulerian framework, but it is still useful to explore this extreme case and contrast the results with those from discontinuous elements or other methods. The original Hibler’s VP rheology was proposed for relatively coarse meshes. While this rheology is not necessarily the best approach in this case, the scales below, which it fails, are not clear yet, and we hope it is still giving some approximation to real dynamics. In our future model development, we will consider testing different sea

ice rheology and model discretization (e.g., Rampal et al. 2019) and incorporate other types of sea ice model formulations (e.g., discrete element method, West et al. 2022). In this regard, our current experience with the traditional sea ice dynamics will provide us with the basic knowledge as a reference for future model improvement.

To this end, we added an estuary (Duluth harbor and the St Louis River) to the previous mesh. St Louis River (Fig. 15) is one of the largest tributaries of Lake Superior,

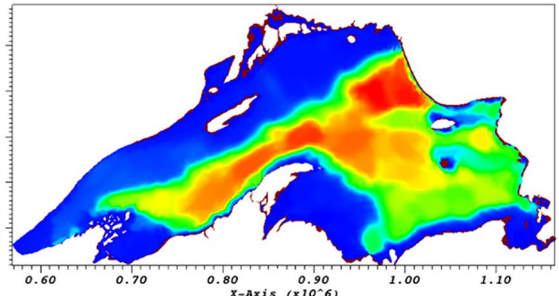
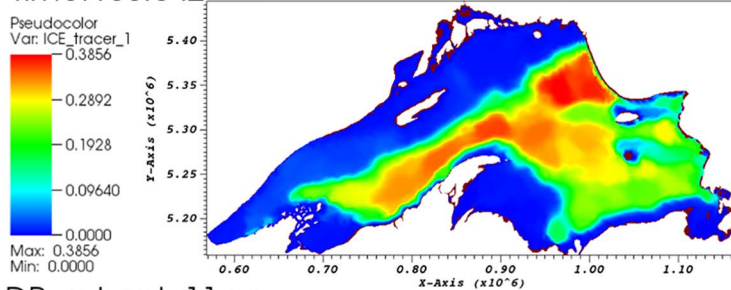
Fig. 12 Ice velocity on March 11, 2019



DB: schout_11.nc
Time: 100,042

(a) Ice mass (m)

(b) Ice mass (m)



DB: schout_11.nc
Time: 100,042

(c) Δ (1/sec)

(d) Δ (1/sec)

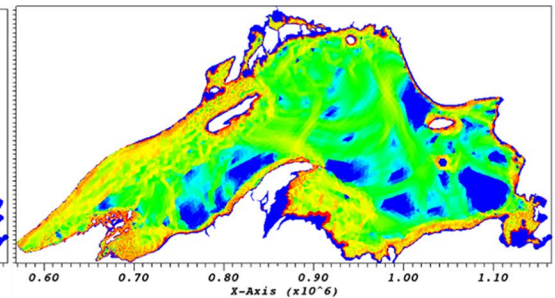
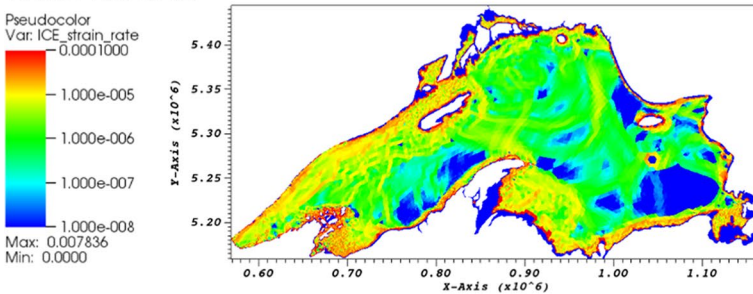


Fig. 13 Sensitivity results from changing α, β in mEVP. **a, c** ice mass and Δ predicted with $\alpha = \beta = 200$; **b, d** ice mass and Δ predicted with adaptive α with $C=200, B=0.01$ (note the minor difference in Δ in the southeast). Similar to Fig. 11, the places where we see some

patchiness in Δ are the places where ice thickness is small (and the concentration is low). This indicates that numerical stability is likely sufficient

Fig. 14 Sensitivity results with respect to the initial condition for temperature. **a** Ice area; **b** averaged ice thickness

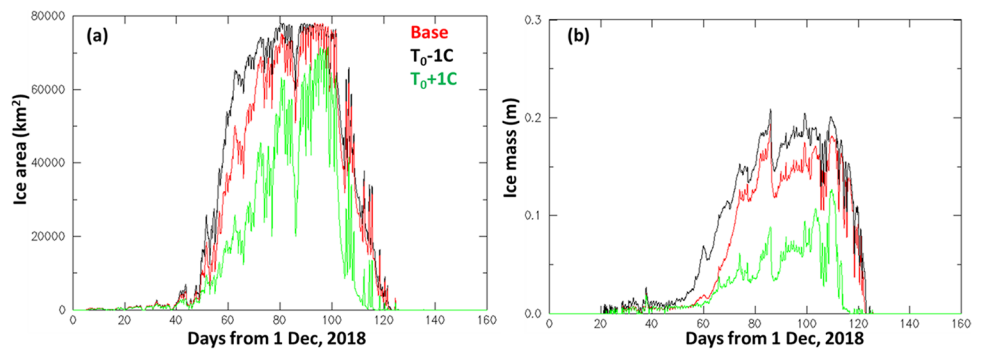
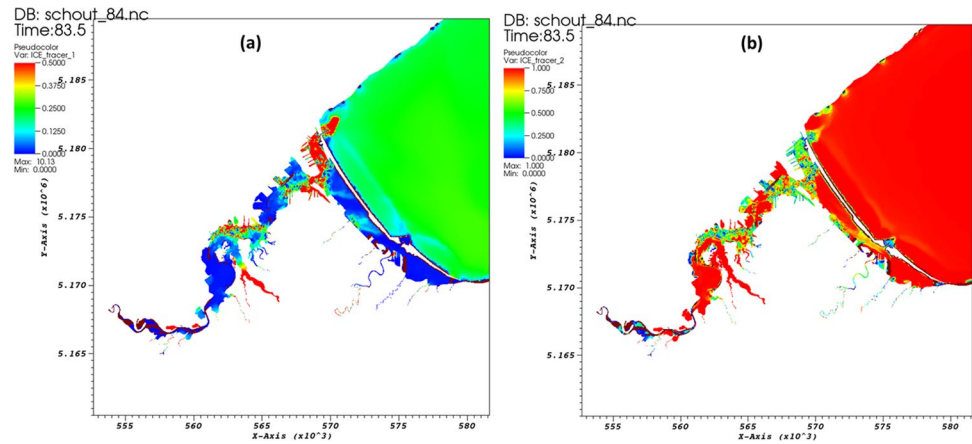


Fig. 15 **a** Ice mass and **b** concentration near Duluth harbor on Feb. 21, 2019. See Supplemental Material for an animation



with an average flow of $\sim 140 \text{ m}^3/\text{s}$. The St Louis watershed also includes other smaller rivers as shown in Fig. 15, and the total discharge from those smaller rivers is roughly 1/3 of St Louis River flow. The unstructured mesh for this system resolves the St Louis watershed and all major bathymetric features like the two entrances to Lake Superior, jetties and boat basins and piers, with resolution down to $\sim 1 \text{ m}$ at many places. This mesh serves as a severe test for both the hydrodynamic and ice model.

The hydrodynamic model setup is the same as before without suffering any instability due to the implicit scheme used. For the ice model, we had to increase the number of iterations for the mEVP solver from 200 to 500 and used an adaptive scheme for α, β , with $C=200, B=0.02$ in Eq. (1) to satisfy the CFL criterion. The maximum number of subcycling in the FCT transport solver is also increased to 40 in order to satisfy the Courant condition (i.e., with a reduced time step for the transport equation). These changes only lead to a moderate increase of $\sim 6\%$ in the computational cost because only one class of ice and snow is used here; with multi-class ice and snow, the increase in the computational cost can be substantial.

The simulated ice field seems reasonable, with the harbor and rivers frozen as the rest of Lake, and no obvious artifacts observed (Fig. 15). The ice may be too thin based on anecdotal observation, but more rigorous validation is necessary in the future when more ice observation is available inside the harbor.

Although the work here shows promises for simulating ice on very localized scales, future work is clearly needed to account for some missing processes: heat exchange between soil and water (which is important for small semi-enclosed systems; Hsieh 2011); wave effects on ice; and landfast ice (Lin et al. 2022); etc. New classes of ice models might be required to address some of these challenges. From a modeling point of view, although the explicit methods (mEVP and advection) appeared to be applicable on

such variable fine meshes as demonstrated in this paper, it remains unclear if we should invest in implicit (or even hybrid explicit-implicit) VP solver and implicit advection, which might require less tuning in the end. An efficient solver and preconditioner for such variable meshes are the key focus for future work. This approach may be able to further smooth the noise in the Δ field.

5 Conclusion

We have successfully developed and validated a simple ice model embedded inside a 3D hydrodynamic model on unstructured grids. The model was able to reasonably capture the ice fields observed in two lakes but slightly overestimated the ice melting speed. For the first time, we attempted simulation of ice processes on very small scales (down to 1 m), although more rigorous validation nearshore is needed. Future work will focus on developing new capabilities for accurately simulating nearshore ice.

Acknowledgements Simulations used in this paper were conducted using the following computational facilities: (1) William & Mary Research Computing (URL: <https://www.wm.edu/it/rc>); (2) Texas Advanced Computing Center (TACC), The University of Texas at Austin.

Funding This study is funded by NOAA (Grant number NA21NOS0080197).

Data availability The datasets generated during and/or analyzed during the current study are available from the corresponding author on reasonable request.

Declarations

Competing interests The authors declare no competing interests.

Supplemental Material An animation of the modeled ice concentration shown in Fig. 8 can be found at http://ccrm.vims.edu/yinglong/TMP/anim_r61f_iceconc.avi (starting day is 1 Dec 2018). An animation of the modeled ice concentration shown in Fig. 15 can be found at http://ccrm.vims.edu/yinglong/TMP/anim_iceconc_r62c.avi.

References

- Anderson J, Liu Y, Moghimi S, Zhang Y, Wu CH (to be submitted) Coastal upwelling and downwelling near the Keweenaw Peninsula, Lake Superior. *J Geophys Res Oceans*
- Bai P, Wang J, Chu P, Hawley N, Fujisaki-Manome A, Kessler J, Lofgren BM, Beletsky D, Anderson EJ, Li Y (2020) Modeling the ice-attenuated waves in the Great Lakes. *Ocean Dyn* 70:991–1003
- Benjamin SG, Smirnova TG, James EP et al (2022) Inland lake temperature initialization via coupled cycling with atmospheric data assimilation. *Geosci Model Dev* 15(17):6659–6676
- Bouchat A, Hutter N, Chanut J, Dupont F, Dukhovskoy D, Garric G et al (2022) Sea ice rheology experiment (SIREx): 1. Scaling and statistical properties of sea-ice deformation fields. *J Geophys Res Oceans* 127:667. <https://doi.org/10.1029/2021JC017667>
- Bouillon S, Fichetef T, Legat V, Madec G (2013) The elastic–viscous–plastic method revisited. *Ocean Model* 71:2–12. <https://doi.org/10.1016/j.ocemod.2013.05.013>
- Bouillon S, Rampal P (2015) Presentation of the dynamical core of neXtSIM, a new sea ice model. *Ocean Model* 91:23–37. <https://doi.org/10.1016/j.ocemod.2015.04.005>
- Fujisaki A, Wang J, Bai X, Leshkevich G, Lofgren B (2013) Model-simulated interannual variability of Lake Erie ice cover, circulation, and thermal structure in response to atmospheric forcing, 2003–2012. *J Geophys Res Oceans* 118:4286–4304. <https://doi.org/10.1002/jgrc.20312>
- Hsieh Y-F (2011) Modeling ice cover and water temperature of Lake Mendota. PhD Thesis. Madison, Wisconsin. University of Wisconsin-Madison
- Hunke EC, Lipscomb WH, Turner AK, Jeffery N, Elliott S CICE (2015) The Los Alamos sea ice model documentation and software user's manual version 5.1, Tech. Rep., Los Alamos National Laboratory, LA-CC-06-012, <https://github.com/CICE-Consortium/CICE-svn-trunk/blob/main/cicedoc/cicedoc.pdf> (last access: 4 April 2022)
- Hutter N, Losch M (2020) Feature-based comparison of sea ice deformation in lead-permitting sea ice simulations. *Cryosphere* 14:93–113. <https://doi.org/10.5194/tc-14-93-2020>
- Kimmritz M, Losch M, Danilov S (2017) A comparison of viscous–plastic sea ice solvers with and without replacement pressure. *Ocean Model* 115:59–69. <https://doi.org/10.1016/j.ocemod.2017.05.006>
- Kitchell JF (1992) Food web management : a case study of Lake Mendota, Lake Mendota Symposium, Madison, Wisconsin. Springer-Verlag, Berlin
- Li Y, Beletsky D, Wang J, Austin JA, Kessler J, Fujisaki-Manome A, Bai P (2021) Modeling a large coastal upwelling event in Lake Superior. *J Geophys Res Oceans* 126. <https://doi.org/10.1029/2020JC016512>
- Lin Y, Fujisaki-Manome A, Anderson EJ (2022) Simulating landfast ice in Lake Superior. *J Mar Sci Eng* 10:932
- Matheson DH, Munawar M (1978) Lake Superior Basin and its development. *J Great Lakes Res* 4(3–4):249–263. [https://doi.org/10.1016/S0380-1330\(78\)72196-9](https://doi.org/10.1016/S0380-1330(78)72196-9)
- Mironov D, Heise E, Kourzeneva E, Ritter B, Schneider N, Terzhevik A (2010) Implementation of the lake parameterisation scheme FLake into the numerical weather prediction model COSMO. *Boreal Environ Res* 15:218–230
- Parkinson CL, Washington WM (1979) A large-scale numerical model of sea ice. *J Geophys Res* 84(C1):311–337. <https://doi.org/10.1029/JC084iC01p00311>
- Rampal P, Dansereau V, Olason E, Bouillon S, Williams T, Korosov A, Samaké A (2019) On the multi-fractal scaling properties of sea ice deformation. *Cryosphere* 13:2457–2474. <https://doi.org/10.5194/tc-13-2457-2019>
- Smirnova TG, Brown JM, Benjamin SG, Kenyon JS (2016) Modifications to the rapid update cycle land surface model (RUC LSM) available in the weather research and forecasting (WRF) model. *Mon Weather Rev* 144:1851–1865
- Titze D, Austin J (2016) Novel, direct observations of ice on Lake Superior during the high ice coverage of winter 2013–2014. *J Great Lakes Res* 42:997–1006
- Wang Q, Danilov S, Sidorenko D, Timmermann R, Wekerle C, Wang X, Jung T, Schroter J (2014) The finite element sea ice-ocean model (FESOM) v.1.4: formulation of an ocean general circulation model. *Geoscientific Model Dev* 7(2):663–693. <https://doi.org/10.5194/gmd-7-663-2014>
- West B, O'Connor D, Parno M, Krackow M, Polashenski C (2022) Bonded discrete element simulations of sea ice with non-local failure: applications to Nares Strait. *J. Adv Model Earth Syst* 14:e2021MS002614. <https://doi.org/10.1029/2021MS002614>
- White B, Austin J, Matsumoto K (2012) A three dimensional model of Lake Superior with ice and biogeochemistry. *J Great Lakes Res* 30(1):61–71
- Xiao C, Lofgren BM, Wang J, Chu PY (2016) Improving the lake scheme within a coupled WRF-lake model in the Laurentian Great Lakes. *J Adv Model Earth Syst* 8:1969–1985
- Ye F, Zhang Y, Friedrichs M, Wang HV, Irby I, Shen J, Wang Z (2016) A 3D, cross-scale, baroclinic model with implicit vertical transport for the Upper Chesapeake Bay and its tributaries. *Ocean Model* 107:82–96. <https://doi.org/10.1016/j.ocemod.2016.10.004>
- Zeng X, Zhao M, Dickinson RE (1998) Intercomparison of bulk aerodynamic algorithms for the computation of sea surface fluxes using TOGA COARE and TAO data. *J Climatol* 11:2628–2644
- Zhang J, Hibler WD (1997) On an efficient numerical method for modelling sea ice dynamics. *J Geophys Res* 102:8691–8702
- Zhang Y, Ateljevich E, Yu H-C, Wu C-H, Yu JCS (2015) A new vertical coordinate system for a 3D unstructured-grid model. *Ocean Model* 85:16–31
- Zhang Y, Ye F, Stanev EV, Grashorn S (2016) Seamless cross-scale modeling with SCHISM. *Ocean Model* 102:64–81. <https://doi.org/10.1016/j.ocemod.2016.05.002>

Springer Nature or its licensor (e.g. a society or other partner) holds exclusive rights to this article under a publishing agreement with the author(s) or other rightsholder(s); author self-archiving of the accepted manuscript version of this article is solely governed by the terms of such publishing agreement and applicable law.